Aerosol Science and Technology

ISSN: 0278-6826 (Print) 1521-7388 (Online) Journal homepage: http://www.tandfonline.com/loi/uast20

A Numerical Study of the Performance of an Aerosol Sampler with a Curved, Blunt, Multi-Orificed Inlet

Pengfei Gao , Bean T. Chen , Paul A. Baron & Sidney C. Soderholm

To cite this article: Pengfei Gao , Bean T. Chen , Paul A. Baron & Sidney C. Soderholm (2002) A Numerical Study of the Performance of an Aerosol Sampler with a Curved, Blunt, Multi-Orificed Inlet, Aerosol Science and Technology, 36:5, 540-553, DOI: 10.1080/02786820252883784

To link to this article: http://dx.doi.org/10.1080/02786820252883784

Published online: 30 Nov 2010.

Aerosol Science and Technology 36: 540–553 (2002)

Published by Taylor and Francis
0278-6826/02/$12.00 + .00

A Numerical Study of the Performance of an Aerosol Sampler with a Curved, Blunt, Multi-Orificed Inlet

Pengfei Gao,[1] Bean T. Chen,[1] Paul A. Baron,[2] and Sidney C. Soderholm[1]
[1]*National Institute for Occupational Safety and Health, Morgantown, West Virginia*
[2]*National Institute for Occupational Safety and Health, Cincinnati, Ohio*

The purpose of this study was to numerically simulate the performance of an aerosol sampler with a curved, blunt, multi-orificed inlet in order to understand the sampling characteristics of the first prototype of the button personal inhalable aerosol sampler ("button sampler"). Because the button sampler inlet design is too complicated to apply a three-dimensional model, an axisymmetric two-dimensional model was created to be similar in geometry and to simulate the major features of the airflow through the sampler when facing the wind. Particle trajectories were calculated in a variety of wind velocities and were categorized into 5 groups based on their interactions with the curved surface of the sampling plane.

Empirical sampling efficiencies of the button sampler for 3 particle sizes were used to adjust the calculated sampling efficiencies in an attempt to improve the accuracy of the two-dimensional axisymmetric model in accounting for interactions between particles and the surface of the inlet of the button sampler. Sampling efficiencies for other particle sizes were then predicted. The results showed that sampling efficiency decreased with increasing particle size up to approximately 40 μm and then remained virtually unchanged at about 35% up to 100 μm. Although the efficiencies were lower than the American Conference of Governmental Industrial Hygienists' (ACGIH) inhalability curve for larger particles, the pattern of the predicted sampling efficiency was quite similar to the ACGIH inhalability curve. Sampling efficiencies for liquid aerosol particles larger than 15 μm were predicted to be noticeably lower than those for solid particles.

The results also showed that the multi-orificed curved surface played an important role in establishing a pressure drop with desired flow alignment inside the sampler, thus greatly reducing the wind effect and significantly improving the uniformity of particle deposition on the filter. The less uniform deposition found at high wind velocity can be improved by increasing the sampling flow rate.

INTRODUCTION

Over the past 2 decades, several personal samplers have been used in workplaces to monitor occupational exposure to potential airborne hazards for risk assessment (Baron 1998). Depending on the desired size fractions, samplers with different design concepts and collection principles have been fabricated to follow the sampling conventions (ACGIH 1998; ISO 1991). Two significant problems are the variation of aspiration efficiency with wind speed and direction, and the nonuniform particle deposition on the collection filter. Vincent (1989) has shown up to a fivefold difference in aspiration efficiency between 2 identical inlets operating in indoor and outdoor environments. Nonuniform deposition on the collection medium of a sampler could be of concern when the measuring technique requires a representative sample. For instance, when conducting bioaerosol measurements using the microscopic counting method, a nonuniform deposit on the filter surface would result in a potential counting bias in the result. Therefore, the ability to minimize the ambient wind effect and to improve uniformity of particle deposition has been a critical concern in inhalable aerosol sampler design.

In an attempt to reduce the problems associated with currently available samplers, an aerosol sampler, referred to as the button personal inhalable aerosol sampler, was developed for ambient air or personal breathing zone sampling (Kalatoor et al. 1995). As shown in Figure 1, the inlet was formed from a portion of a spherical shell with numerous, identical, evenly spaced orifices. In the first prototype sampler, a metal sheet with a 19% porosity and an orifice diameter of 254 μm was formed into a spherical inlet with a subtended angle of 140°. The thickness of the sheet was 203 μm. A 25 mm polyvinyl chloride (PVC) filter was placed directly after the multi-orificed surface. The flow rate was fixed at 2 L/min, which was readily achieved by using a commercial personal sampling pump. Currently, there

Received 23 August 2000; accepted 16 August 2001.

Mention of product or company names does not constitute endorsement by the Centers for Disease Control and Prevention.

The authors would like to express their appreciation to Drs. Klaus Willeke and Sergey Grinshpun of the University of Cincinnati for providing experimental data that was used for comparison to our numerical results and for valuable discussions; to Dr. Vladimir Hnizdo at the National Institute for Occupational Safety and Health for his help on fitting the numerical data to the experimental results; and to Drs. Matthew Godo and Ashwini Kumar of FLUENT Inc. for support with FIDAP software applications.

Address correspondence to Pengfei Gao, National Institute for Occupational Safety and Health, P.O. Box 18070, Cochrans Mill Road, Pittsburgh, PA 15236. E-mail: pgao@cdc.gov

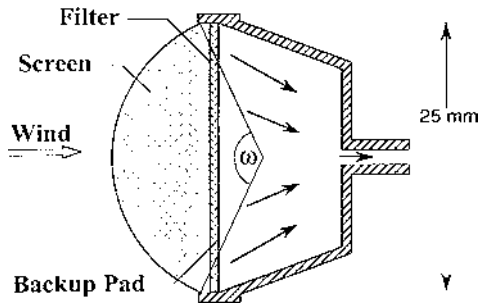

Figure 1. Schematic diagram of the button sampler.

is a commercial version available from SKC Inc. (Eighty Four, PA) that has different inlet characteristics. It has an inlet porosity of 21%, with orifices that are 381 μm in diameter and a recommended sampling flow rate of 4 L/min (Aizenberg et al. 2000).

Laboratory and field tests for stationary and personal monitoring demonstrated that the first prototype button sampler collection efficiency was virtually independent of wind velocity and less affected by wind direction than a 25 mm closed-face filter cassette. Wind tunnel tests using monodisperse particles of uranine (sodium fluorescein) showed that the sampling efficiency varied from about 30% for 38 μm particles to approximately 50% for 17 μm particles when the sampler faced the wind. The sampler, using a multi-orificed surface, reduced the number of particles collected that were >100 μm. Nonuniformity of filter deposition for this sampler was found to be less than half that for the closed-face 25 mm filter cassette when facing the wind. The uniformity for a 45° yaw angle was also superior (Kalatoor et al. 1995; Hauck et al. 1997). Airflow and particle velocity patterns in the vicinity of the sampler have also been determined using laser-doppler velocimetry (LDV) in a wind tunnel (Aizenberg et al. 1998). The LDV results showed that nondimensionalized airflow patterns and particle-velocity fields near the curved surface were similar at different wind velocities when facing the wind. The measurements also demonstrated that the presence of a stagnation plate simulating the human torso did not induce a significant change in airflow and particle trajectory profiles near the inlet when it faced the wind and the distance from the stagnation plate was greater than the sampler diameter. The sampling efficiency of the commercial sampler was found not to depend significantly on its orientation to the wind when mounted on a manikin (Aizenberg et al. 2000). A recent study demonstrated that the sampler was suitable for total and viable enumeration of airborne microorganisms (Grinshpun et al. 2000).

The motivation for conducting this study was to reveal the physical mechanisms of the performance of such an aerosol sampler using computational fluid dynamics (CFD). In the field of aerosol science, CFD has been used in estimating the particle deposition in the respiratory tract (Li et al. 1998; Katz et al. 1999), the aerosol concentration in ventilated workplaces (Kulmala 1997), particle-wall interactions (Tu 2000), and collection efficiency in samplers (Griffiths and Boysan 1996; Twohy 1998; Gao et al. 1999). Because of the complex inlet geometry of the button sampler, our approach was to use an axisymmetric, two-dimensional CFD model as a numerical approximation. As pointed out by Wilck and Stratmann (1997), it is strongly desirable to acquire CFD models in aerosol science that are sufficiently simple in order to be applied in complex geometry and still yield reliable information on the basic properties of the resulting flow field and particle trajectory. Examples include the modal aerosol dynamics modeling technique (Whitby 1989) and the two-dimensional multicomponent modal aerosol model for an aerosol reactor (Wilck and Stratmann 1997).

In this study, the commercially available, finite-element-based fluid flow simulation program FIDAP (FIDAP 7.62, Fluent, Inc., Lebanon, NH) was used to simulate the airflow through the first prototype button sampler and to calculate the particle trajectories. Physical mechanisms of the sampler's performance were numerically investigated. Particle trajectories were categorized into 5 groups based on their interactions with the multi-orificed sampling plane. Sampling efficiencies obtained by numerical simulation were compared with available empirical data (Kalatoor et al. 1995) so that interactions between particles and the blunt surface (i.e., the curved surface of the inlet exclusive of the holes) could be approximated and corrected. In addition, sampling efficiencies for more particle sizes ranging from 5 to 100 μm were numerically predicted for comparing with the American Conference of Governmental Industrial Hygienists' (ACGIH) inhalability curve (Soderholm 1989; ACGIH 1998).

SIMULATION PROCEDURES

Creating the Geometry and Mesh for the Computational Domain

As shown in Figure 1, there were hundreds of tiny holes across the curved surface of the button sampler, so creating a three-dimensional full CFD model was extremely complicated. It was estimated that even one-sixth of its full geometry requires approximately 750,000 nodes for mesh generation, which demands 1.0 Gbyte of memory in the current FIDAP version. Therefore, an axisymmetric, two-dimensional CFD model was created as a simplified and feasible approach. While this greatly simplified the geometry and mesh setup, it created a less realistic approximation. As a result, the numerical model treated each orifice on the curved inlet as a circular slit, and the sampler orientation was facing the wind only. After requiring the orifices to be evenly spaced and 254 μm wide, the desired 19% porosity was achieved using 12 orifices. As shown in Figure 2, a total of 14,822 nodal points that contain 15,661 elements defined the computational domain for all wind conditions. More than three quarters of the total mesh was distributed around and within the sampling orifices, where the flow fields are more interesting and have a greater impact on sampling efficiency. Calculations of the flow field at a greater number of nodal points did not seem to be justified. Increasing the number by 20% changed velocities

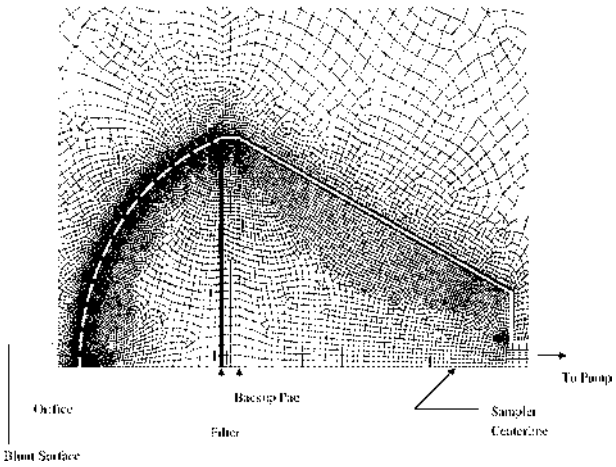

Figure 2. Mesh distribution in the region around the multi-orificed inlet.

by <2% and did not significantly change sampling efficiencies. A torso was not included in the CFD model, similar to the wind tunnel tests (Kalatoor et al. 1995).

Defining the Permeability of the PVC Filter for the CFD Model

FIDAP required a permeability parameter when a filter was included in the model. A PVC filter was used during the empirical evaluation of the sampler. Pressure drops through the filter had an impact on the flow field around the filter surfaces, thus affecting the uniformity of particle deposition. According to the filter manufacturer, the thickness of the PVC filter was 0.01 cm with a porosity of 70%; pressure drop (ΔP) for air through the filter was 10.16 cm of water at an average superficial velocity of 3.33 cm/s, i.e., $\Delta P = 10.16\ \text{cm} \times 1.00\ \text{g/cm}^3 \times 981\ \text{cm/s}^2 = 9{,}967\ \text{g/cm/s}^2$. Hence

$$\begin{aligned}\text{Permeability} &= u_x \times \Delta x \times \frac{\nu}{\Delta P} \\ &= 3.33\ \text{cm/s} \times 0.01\ \text{cm} \times \frac{0.00018\ \text{g/cm/s}}{9967\ \text{g/cm/s}^2} \\ &= 6.0 \times 10^{-10}\ \text{cm}^2, \end{aligned} \quad [1]$$

where u_x, Δ_x, and ν are average velocity, thickness of the filter, and viscosity of the air, respectively.

Computing the Flow Field

FIDAP uses the finite element method to simulate many classes of fluid flow. The principal governing equations for fluid flow and mass transfer that are solved by FIDAP include the continuity equation (conservation of mass) and the Navier–Stokes equations (conservation of momentum) and conservation of energy (Engelman 1993). A uniform velocity field at the inlet of the computation domain was specified. Velocities at the walls were set to be zero, and outlet pressure was set to be the same as the ambient pressure. The assumption was also made that the modeled particle concentrations were dilute enough to avoid interactions among particles. Preliminary studies showed that turbulence did not significantly affect the results. This was because the mesh was sufficiently dense and the Reynolds numbers were <10,000. Computations were performed at wind velocities ranging from 1.0 to 3.0 m/s in an increment of 0.5 m/s in order to compare them to the empirical results (Kalatoor et al. 1995). Additionally, wind velocities of 0.5 and 4.0 m/s were simulated not only for comparisons to the flow fields that were determined using LDV (Aizenberg et al. 1998) but also because they represent typical indoor and outdoor environmental conditions, respectively (Berry and Froude 1989). For all the simulations, the sampling flow rate was fixed at 2 L/min, except for the wind velocity of 4.0 m/s for which the sampling flow rate of 10 L/min was also simulated. Each simulation converged after 25 iterations. An interval between residuals of the resulting i and $i+1$ values was set to be $\pm\ 1e{-}06$.

Calculating Particle Trajectories

After the flow fields were simulated, the prediction of particle trajectories was determined by the Lagrangian formulation of particle motion:

$$\frac{du_p}{dt} = F_D(u - u_p) + g_x \frac{(\rho_p - \rho)}{\rho_p}, \quad [2]$$

where the left side of the equation represents the particle acceleration and therefore represents the force applied per unit particle mass according to Newton's second law ($a = F/m$). μ and μ_p are the molecular viscosities of the fluid and particles, and ρ and ρ_p are the densities of the fluid and particles, respectively. $F_D(\mu - \mu_\rho)$ is drag force per unit particle mass, and $g_x\ (\rho_p - \rho)/\rho_p$ is the gravitational force per unit particle mass.

The "implicit" keyword (Implicit = 20) was selected for a semi-implicit solver where the derivatives were evaluated at time level n as well as at time level $n+1$. The "variable" keyword (Variable = $1.0e{-}05$) was selected that allowed the implicit solver to exert some adaptive control over its own progress—the technique used was "step doubling." FIDAP takes each step twice, once as a full step, then independently as 2 half steps. The values of the DTMAX (maximum time increment for path computation) and the DTMIN (minimum time increment for path computation) were set to be $5.0e{-}03$ and $1.0e{-}07$, respectively. The value of DT (time increment for path computation) was set to be $1.0e{-}06$ s.

The surface of the screen inlet of the sampler was defined as "not sticky" because dry and solid aerosol particles were used in the wind tunnel tests for the 3 particle sizes. This allowed for particle bounce and reentry to the flow after impacting the wall, so the final fate of each particle trajectory through the entire computation domain could be observed. The ratio of the rebounding velocity to the incident velocity (i.e., coefficient of restitution) was specified to be 80% according to other investigators

(Wall et al. 1990). The current FIDAP version assumes that the rebounding angle of a particle is the same as its incident angle, the particle is spherical, and no heat or mass is exchanged between the particle and the surface of the sampling inlet.

Sampling efficiencies for the particle sizes of 17, 26, and 38 μm were simulated to compare with the available experimental data (Kalatoor et al. 1995), while sampling efficiencies for 5 additional particle sizes (i.e., 5, 10, 50, 70, and 100 μm) were predicted to cover the entire range of the ACGIH inhalabitity curve. A number of particles at each particle size were released into the upstream wind to determine the limiting trajectory. Outside the limiting trajectory envelope, a particle would have no chance to interact with the sampler's surface. The distance between the starting point of the limiting trajectory and the symmetric line of the sampler was divided into 10 equal increments. Twenty monodisperse aerosol particles were uniformly released 10 cm upstream of the sampler within each increment, and a total of 200 particles determined the sampling efficiency for each particle size at a given wind velocity. Doubled the particles did not significantly affect the sampling efficiencies. In reality, if the distance of the particle center to the orifice edge is less than the radius of the particle, the particle will likely hit the wall. Numerically, the particle does not have a finite dimension. Even if the particle is infinitesimally close to the edge but not exactly on it, it will pass through the orifice. This effect was taken into account when observing the particle trajectories as mentioned below.

Calculating Sampling Efficiencies from the Particle Trajectories

Sampling efficiencies were calculated according to the detailed particle trajectory information. Particle trajectories were categorized into 5 groups: (A) particles that directly passed through an orifice without hitting a wall, (B) particles that passed within one particle radius of an orifice's internal wall, (C) particles that hit on a blunt surface between orifices and then bounced at least once and then passed through an orifice onto the filter, (D) particles that impacted a blunt surface and stayed or bounced one or more times onto another blunt surface, and (E) particles that hit on a blunt surface between orifices and then bounced at least once and bypassed the sampler.

Since the experimental data were obtained using solid particles, it was presumed that (1) all the particles in groups A and B were collected on the filter, (2) there was a fraction (k_1) of the group C particles that could really enter into an orifice and be collected on the filter, (3) there was a fraction (k_2) of the group E particles that could really bypass the sampler and thus the remaining ($1-k_2$) could enter into an orifice and be collected on the filter, and (4) group D did not have a chance to be collected on the filter. Although particles in the group B impact on the surface inside the orifice, all the particles were likely to be bounced by other particles and eventually reentrained into the adjacent flow streams into the sampler. In this study, the parameters k_1 for group C and k_2 for group E particles were needed because of the differences in orifice distribution and the roughness of the wall between the button sampler and the numerical model. Values of k_1 and k_2 were estimated by companions with the available empirical data as described later.

The fraction of particles that could be collected on the filter, f_i, was calculated as follows:

$$f_i = \frac{A + B + k_1 C + (1 - k_2)E}{A + B + C + D + E}, \quad [3]$$

where A, B, C, D, and E are particle numbers in each group, as defined above. The subscript "i" refers to different radial zones.

The predicted sampling efficiency of a three-dimensional axisymmetric sampler represented by the two-dimensional simulation was calculated as outlined below. The number of particles (n_{0i}) that would pass through each radial increment ($r_i - r_{i-1}$) can be expressed as a function of air velocity (V_{air}), particle number concentration (C_0) in the upstream air, duration of the experiment t, and the cross-sectional area of the increment.

$$n_{0i} = V_{\text{air}} t C_0 \pi \left(r_i^2 - r_{i-1}^2\right). \quad [4]$$

The number of particles collected in each radial increment (n_{si}) was

$$n_{si} = n_{0i} f_i. \quad [5]$$

The total number of particles that was released (N_0) and the total number of particles that was collected (N_s) were thus calculated using Equations (6) and (7), respectively.

$$N_0 = V_{\text{air}} t C_0 \pi \sum_{i=1}^{10} \left(r_i^2 - r_{i-1}^2\right), \quad [6]$$

$$N_s = \sum_{i=1}^{10} n_{0i} f_i = \sum_{i=1}^{10} f_i V_{\text{air}} t C_0 \pi \left(r_i^2 - r_{i-1}^2\right). \quad [7]$$

Sampling efficiency (η) was then calculated as follows:

$$\eta = \frac{N_s}{N_0} = \frac{\sum_{i=1}^{10} f_i V_{\text{air}} t C_0 \pi \left(r_i^2 - r_{i-1}^2\right)}{V_{\text{air}} t C_0 \pi \sum_{i=1}^{10} \left(r_i^2 - r_{i-1}^2\right)}$$

$$= \frac{\sum_{i=1}^{10} f_i \left(r_i^2 - r_{i-1}^2\right)}{r_{10}^2 - r_0^2}$$

$$= \frac{\sum_{i=1}^{10} f_i \left(r_i^2 - r_{i-1}^2\right)}{r_{10}^2}, \quad [8]$$

where r_0 in Equation (8) equals zero. Note that the value of i ranges from 1 to 10 since there were 10 increments.

RESULTS AND DISCUSSION

Flow Field around the Sampler

Sampling at 0.5 m/s Wind Velocity. Figure 3 illustrates the simulated flow fields around the sampler when sampling in wind with a velocity of 0.5 m/s. Figure 3a is a plot for the velocity vector field, and the corresponding pressure contour plot is given in Figure 3b. Figure 3a shows that the airflow was generally smooth near the curved surface, as was observed experimentally using an LDV (Aizenberg et al. 1998). Except for the axis of the sampler, vectors upstream diverged as they approached the curved surface. The magnitude of the flow

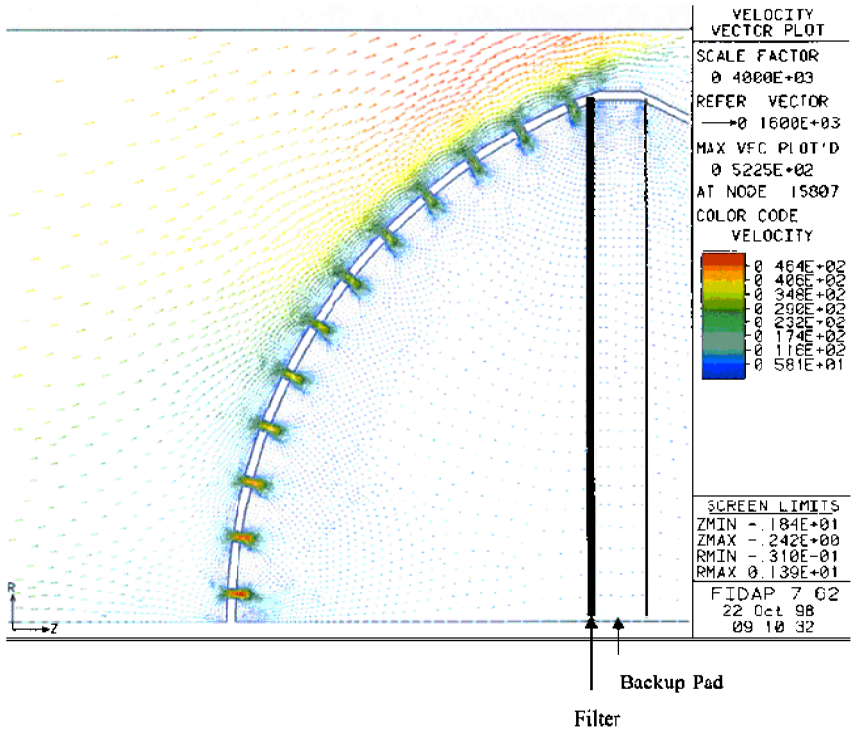

(*a*)

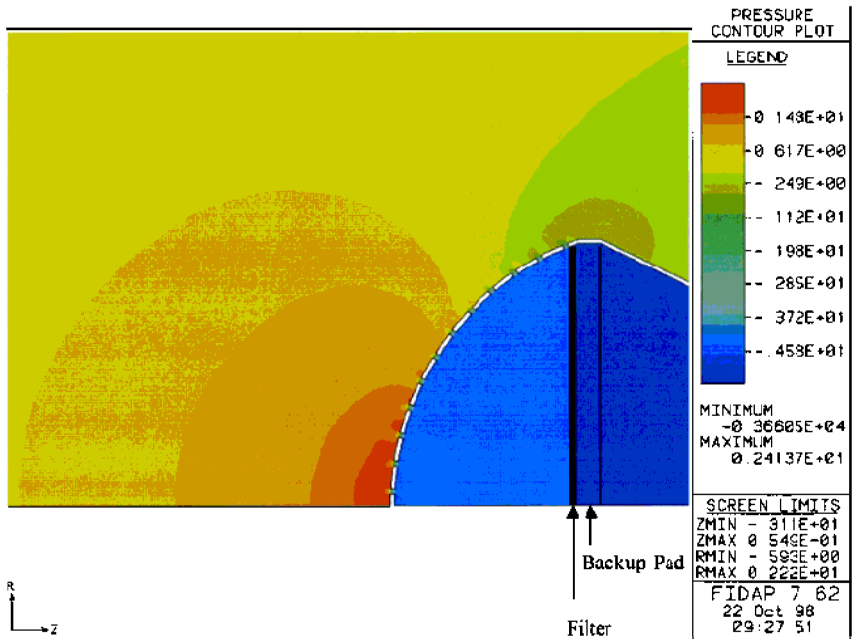

(*b*)

Figure 3. Flow field when sampling at a wind velocity of 0.5 m/s and a sampling flow rate of 2 L/min. (a) Velocity vector field (cm/s). (b) Pressure contour plot (dyn/cm^2).

divergence increased with increasing distance from the axis of the sampler.

Airflow through the orifices was not perfectly uniform; the velocities through the orifices had a coefficient of variation of 17.4%. In general, the sampling velocity was the highest in the orifice near the center of the multi-orificed surface and decreased with increasing distance away from the center. The blunt surface between the orifices caused air streams to merge with each other and change direction to fit into the sampling flow pattern immediately after passing through the multi-orificed surface. This produced a virtually uniform flow distribution near the filter and significantly reduced air velocity inside the sampler. According to Rao et al. (1993), particles tend to focus toward the center in a straight nozzle, which may result in their enrichment near the axis of the nozzle. As shown in Figure 3b, although the pressure on the curved surface was extremely nonuniform as a result of the development of the radial flow on the upstream side, pressure inside the sampler was approximately uniform due to the existence of the multi-orificed surface, which tended to equalize the pressure drop.

Sampling at 2.0 m/s Wind Velocity. Wind velocity at 2.0 m/s was the median value for the various wind velocities simulated. The flow field around the sampler at this wind velocity is shown in Figure 4. Figure 4a is the detailed velocity vector field, and Figure 4b is the corresponding pressure contour plot. The flow pattern was generally similar to that observed in the previous case. However, the increased wind velocity had a greater impact on the airflow distribution through the orifices with a coefficient of variation of the velocities being 93.7%. Due to the higher velocity pressure around the center of the curved surface, the pressure distribution inside the sampler was not as uniform as that observed in the previous case. As shown in Figure 4b, the pressure was higher inside the sampler than outside for the orifices at the 2 outermost positions, causing flow out of the sampler. Although flow streams merged with each other quite well immediately after passing the orifices, the velocity had a large radial component when approaching the filter due to the higher pressure that existed around the axis of the sampler.

Sampling at 4.0 m/s Wind Velocity. The flow pattern around the sampler when sampling at a wind velocity of 4.0 m/s is depicted in Figure 5. As shown in Figure 5a, the flow pattern was generally similar to the 2 previous cases and the airflow was generally smooth near the multi-orificed surface as observed by LDV (Aizenberg et al. 1998). Because the pressure upstream of the sampler around the center of the curved screen (as shown in Figure 5b) was much higher than those in the previous 2 cases (50.2 and 3.9 times according to the CFD results, respectively), the airflow distribution through the orifices was less uniform with a coefficient of variation of the velocities being 140.3%. Inside the sampler, the pressure gradient (higher in the region around the centerline of the sampler and lower in the region near the edge) forced the velocity vector radially. As shown in Figure 5b, the outflow occurred for the 3 outmost positions. Therefore, only relatively few particles were collected through the outer edge orifices and the majority of aerosol particles deposited on the filter were collected through the orifices around the central area of the inlet surface. This effect was discussed by Aizenberg et al. (1998) and was referred to as a "limited transparency of the inlet surface" of the button sampler. It is thus postulated that less uniform particle deposition would be obtained in outdoor environments where high wind velocity is usually encountered. This problem could be remedied by increasing the sampling flow rate, as shown in Figure 5c. When sampling at 10.0 L/min, phenomenon of the outflow disappeared. The pressure distribution inside the sampler was quite uniform and generally lower than the pressure on the upstream side of the sampler (Figure 5d). It can be assumed that the airflow inside the sampler would actually be more uniform than that found in the numerical simulations, since the curved sampling surface with the tiny holes in the actual button sampler would create a more even pressure drop than the circular slits in this simplified numerical model.

Particle Trajectories and Particle-Wall Interaction

FIDAP uses the Lagrangian approach to simulate the particle-wall interaction and the motion of a particle in the flow field. The motion of a particle is determined by local aerodynamic forces. In the particle path plot, the path of particle motion is tracked based on the computed flow field. The position of the particle is plotted at each specified time increment between a given start and end time. Unlike the commonly encountered sampling inlets, such as tubular or circular slit inlets that do not have blunt surfaces within the sampler opening, the inlet of the simulated sampler contains 81% blunt surface (Kalatoor et al. 1995). Therefore there were special aspects in this study that needed to be carefully derived because all have significant influences on particle trajectories and thus the sampling efficiencies. These included the interaction between the particles and the blunt surface within the inlet plane and the particle's velocity after it impacts on the blunt surface. This particle velocity is determined by the coefficient of restitution.

Calculated particle trajectories approaching the blunt surface and inside the sampler are illustrated in Figure 6 at various wind and sampling velocities. Different colors in the figures distinguish the trajectories of different particles (a range of 128 colors varying continuously from blue through red, then repeated). As can be seen in Figures 6a and b, particles with a small Stokes number (Stk = 0.04 and 0.18, respectively) followed the gas streamlines generally quite well and rarely collide with the wall. For a larger Stokes number of 1.4, many particles impacted the blunt surface and bounced some distance, as shown in Figures 6c and d. Such a distance has been referred to as "particle rebound distance," X_{prd}, or particle rebound layer by Tu (2000). Increasing the sampling flow rate from 2 to 10 L/min did not make a noticeable change in the particle rebound layer, when comparing Figures 6c and d. As a result of particle rebound, the particulate concentration increased near the edge of the particle rebound layer due to the reflected particles that moved very slowly there. Tu (2000) reported that concentration near the edge

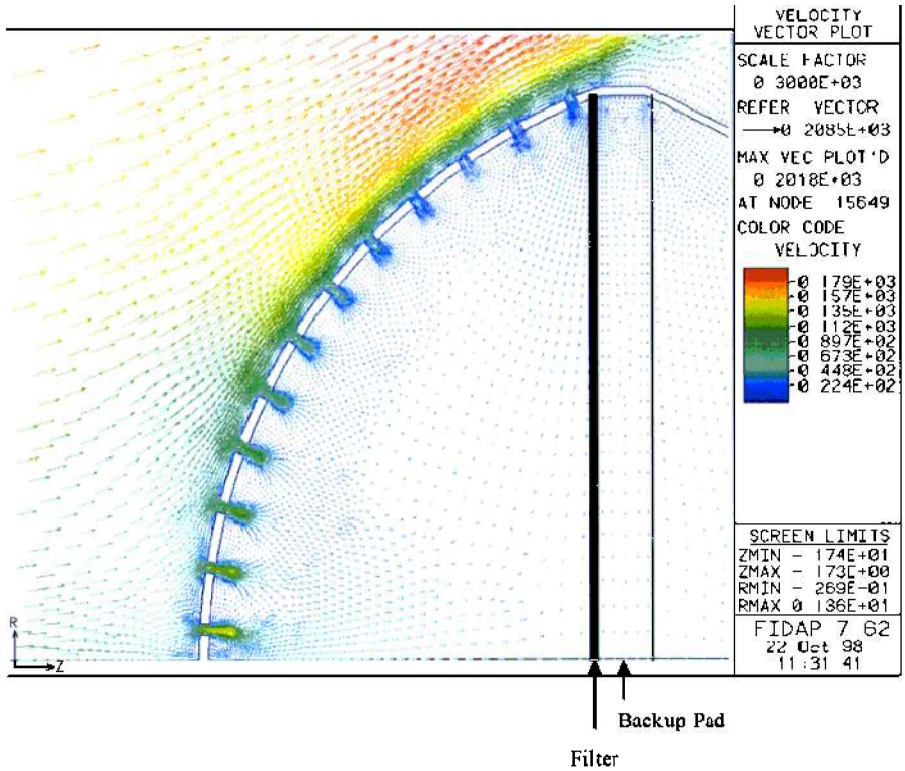

(*a*)

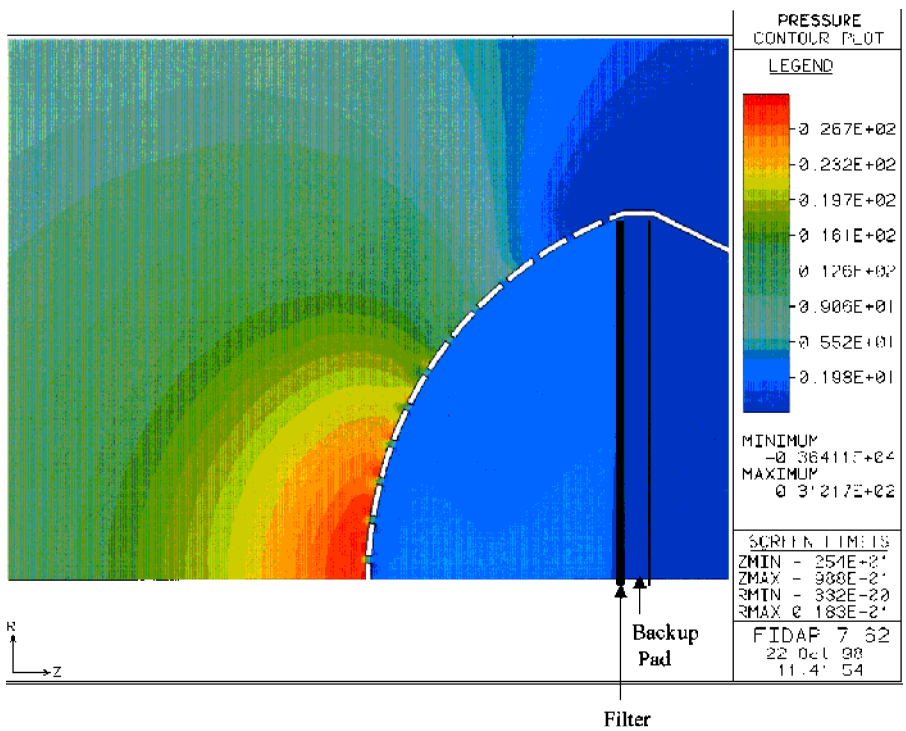

(*b*)

Figure 4. Flow field when sampling at a wind velocity of 2.0 m/s and a sampling flow rate of 2 L/min. (a) Velocity vector field (cm/s). (b) Pressure contour plot (dyn/cm^2).

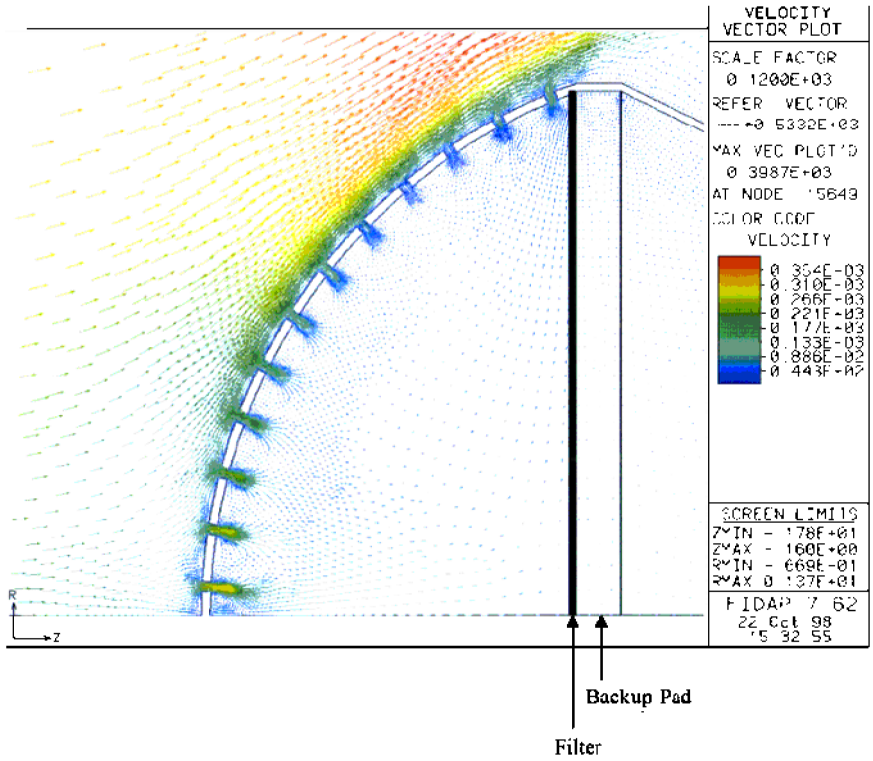

(*a*)

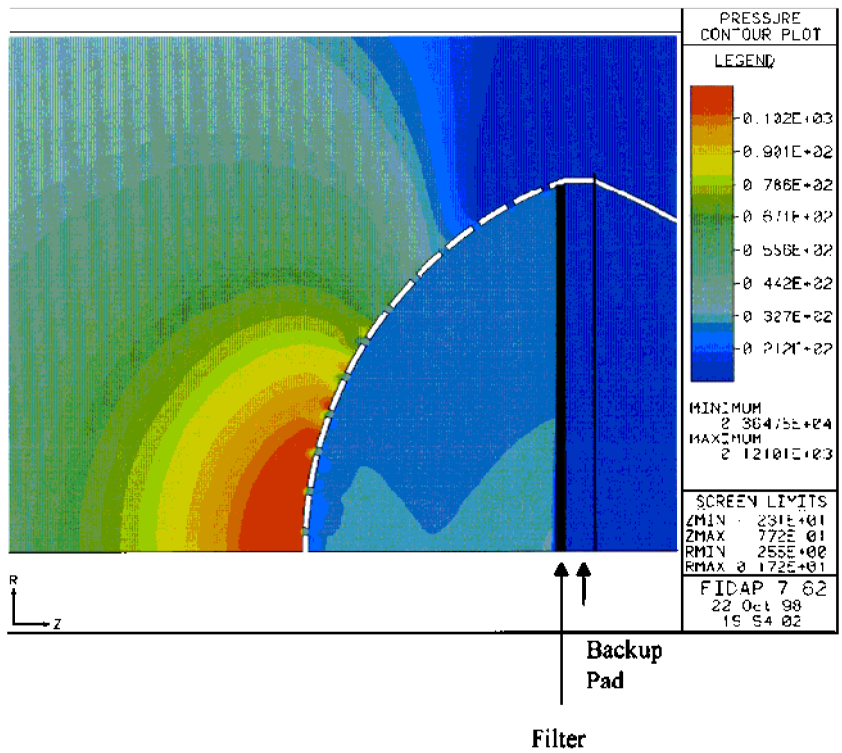

(*b*)

Figure 5. Flow field when sampling at a wind velocity of 4.0 m/s. (a) Velocity vector field (cm/s) at a sampling flow rate of 2 L/min. (b) Pressure contour plot (dyn/cm^2) at a sampling flow rate of 2 L/min. (c) Velocity vector field (cm/s) at a sampling flow rate of 10 L/min. (d) Pressure contour plot (dyn/cm^2) at a sampling flow rate of 10 L/min. *(Continued)*

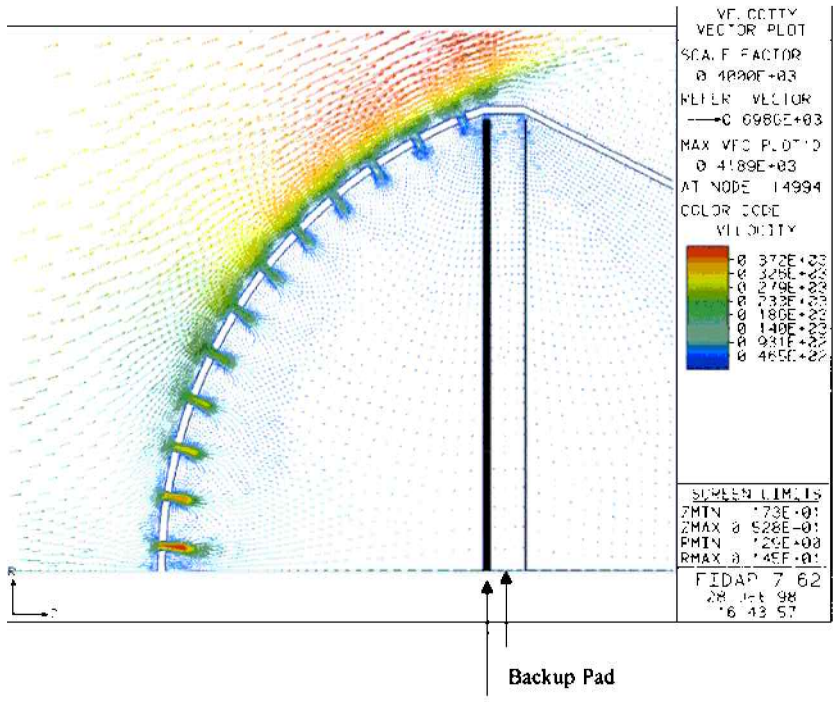

(*c*)

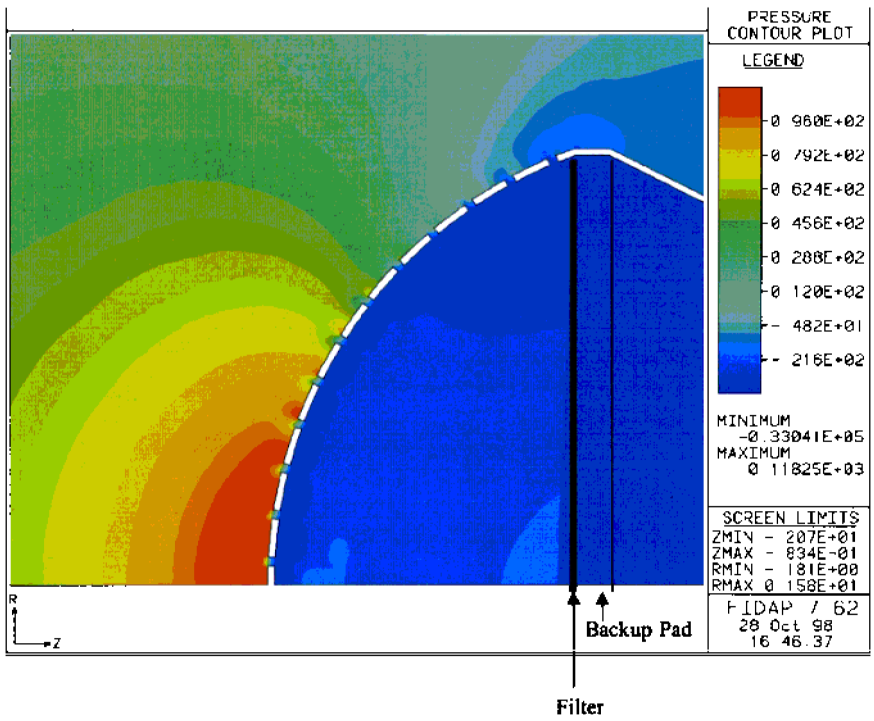

(*d*)

Figure 5. (Continued)

of the particle rebound layer was about 7 times higher than that of the incident particles for Stk = 4 in his study.

The Coefficient of restitution had an effect on sampling efficiency by numerical simulation. In this study, the coefficient of restitution was specified to be 0.8 based on empirical results reported by other investigators (Wall et al. 1990; Brach and Dunn 1998). In fact, the coefficient of restitution depends on a number of factors, such as impact velocity, particle size, material

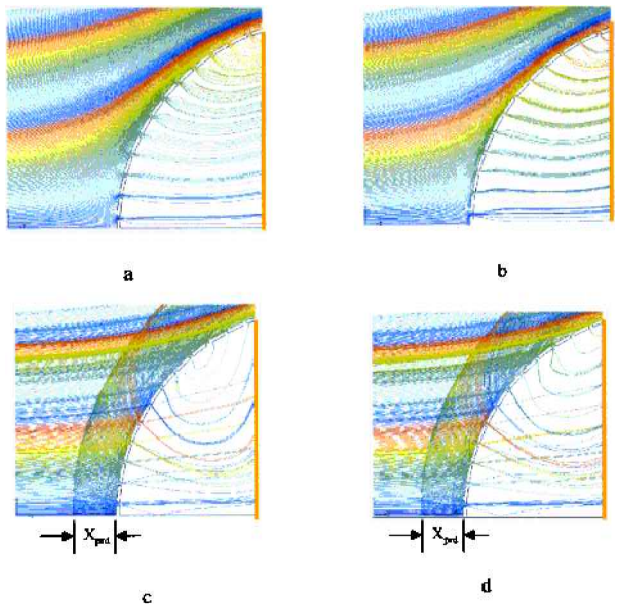

Figure 6. Particle trajectories approaching the blunt surfaces with the sampling plane and inside the filter. (a) A wind velocity of 0.5 m/s and a sampling flow rate of 2 L/min for 17 μm particles (Stk = 0.04). (b) A wind velocity of 0.5 m/s and a sampling flow rate of 2 L/min for 38 μm particles (Stk = 0.18). (c) A wind velocity of 4.0 m/s and a sampling flow rate of 2 L/min for 38 μm particles (Stk = 1.4). (d) A wind velocity of 4.0 m/s and a sampling flow rate of 10.0 L/min for 38 μm particles (Stk = 1.4). X_{prd} is an abbreviation for particle rebound distance. The orange line on the right side of each plot represents the filter.

properties, and roughness of the impact surface and the particle. Brach and Dunn (1998) showed that the coefficient increased with increasing impact velocity but changed insignificantly when the impact velocity was greater than about 1 m/s. They also showed that the coefficient of restitution increased with increasing particle size. At an impact velocity of 1 m/s, the coefficient was about 0.73 for a 70 μm particle and 0.82 for a 140 μm particle (estimated from a figure). Wall et al. (1990) reported that the coefficient of restitution varied from 0.73 to 0.84 when using ammonium fluorescein particles (particle diameter varied from 2.58 μm to 6.89 μm). Since the effect of particle size and impact velocity (when >1 m/s) on the coefficient of restitution was not very significant, and there was no information available on what value to use for the type of particle and surface that were involved in this study, one value of the coefficient (i.e., 0.80) was used based on the available information. Of course, the use of one value of the coefficient of restitution for all the particle sizes and wind velocities is an approximation.

Inside the sampler, particles deposited across the filter quite uniformly, especially for smaller particles at the lower wind velocity shown in Figure 6a ($U_w = 0.5$ m/s, $d_a = 17$ μm). Uniformity generally declined with increasing particle size as shown in Figure 6b ($U_w = 0.5$ m/s, $d_a = 38$ μm) or with increasing wind velocity when comparing Figure 6b to Figure 6c ($U_w = 4.0$ m/s, $d_a = 38$ μm). Figure 6c also reveals that at high wind velocity, a few particles that had passed through the inlet surface escaped with the outflow through the outer edge of the sampler. Larger particles did not follow the outflow due to their high inertia. Although not shown in these figures, the phenomenon occurred when wind velocities reached or were higher than 2 m/min. The problem was remedied by increasing the sampling flow rate, as shown in Figure 6d. This measure also notably improved the uniformity of the deposition. However, sampling efficiencies would change by increasing the sampling flow rate. Therefore, other design parameters of the simulated first prototype button sampler might need to be adjusted in order to follow the inhalable convention more closely. The button sampler demonstrated good filter collection uniformity, but particle deposition was concentrated near the center of the filter when using a standard closed-face cassette (Hauck et al. 1997).

Figure 7 shows a typical particle path plot for particles ($d_a = 50$ μm) that were released upstream at a wind velocity of 2.0 m/s. Of the 20 particles, 11 passed directly through the orifice, 2 hit on the orifice's internal wall, and 7 hit on the blunt surfaces between orifices and then bounced and reentered the flow. As mentioned earlier, these 3 types of trajectories were categorized as groups A, B, and C (or E), respectively, for the calculation of sampling efficiency. At first glance only one particle hit the orifice's internal wall. However, one additional trajectory was categorized in group B because the distance of the particle center to the orifice edge was <25 μm (i.e., one radius of the particle). In reality, this particle would hit the orifice's internal wall. There were not any particles in group D observed in this case.

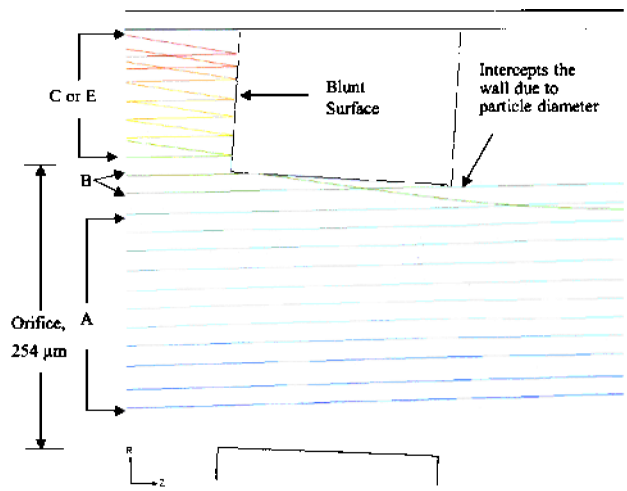

Figure 7. A typical trajectory plot for 50 μm particles when sampling at a wind velocity of 2 m/s and a sampling flow rate of 2 L/min. Group A includes particles that directly passed through an orifice without hitting a wall; group B includes particles that intercept an orifice's internal wall; and group C (or E) includes particles that bounced from a blunt surface between orifices and then reentered the flow inside or outside the sampler.

Detailed information on particle trajectories comprising each of the 5 groups is shown in Figure 8. Figure 8a indicates that approximately 90% of the 5 μm particles were able to follow the gas streamlines and directly pass the orifices. Unlike larger particles, smaller particles were able to make a turn with gas streamlines when approaching the multi-orificed inlet due to their low inertia. The majority of airborne bacteria and fungal spores belong to group A, which would be collected with high efficiency without damage by hitting the blunt surfaces of the inlet. The percentage dramatically dropped to about 15% for diameters near 20 μm and then remained almost the same for larger diameters up to 100 μm.

The phenomenon of outflow, as described earlier, was found in group A particles with relatively small sizes only. Although our presumption that all the particles entering the orifices will be collected on the filter was not always the case, the effect of outflow on calculated sampling efficiencies was negligible, i.e., approximately 0.5% for a wind velocity at 2 m/s and 1.5% for a wind velocity at 4 m/s, when sampling at 2 L/min. However, large particles did not follow the outflow due to their high inertia. In addition, it is evident that group A decreased with an increase of wind velocity between 5 and 20 μm, but the opposite pattern was observed for larger particles. Wind velocity had a larger effect for smaller particles than for the larger ones.

Figure 8b shows the relatively small portion of particles that would be expected to hit an orifice's internal wall (group B), with the highest amounts for diameters between 10 and 17 μm. Basically, particles in group B were able to follow the gas streamlines to the orifices but were unable to make a turn with the streamlines inside the orifices due to higher inertias than group A particles. The percentages were $<7\%$ for diameters >50 μm. Generally, peaks shifted to smaller particle size with increasing wind velocity, but the change was insignificant for wind velocities between 2.0 and 3.0 m/s.

The percentages of particles impacting a blunt surface and then entering an orifice (i.e., group C) or bypassing the sampler (i.e., group E) are presented in Figures 8c and e, respectively. Particles with relatively high inertia in these 2 groups often had multiple impacts. A second impact always occurred much closer to the sampler's edge because of the radial airflow near the blunt surfaces. Rebound velocities for the second or third impaction were significantly lower than for the first impaction since particle velocities normal to the wall were suddenly decreased within the particle rebound distance (PRD in Figures 6c and d). It can be seen that the percentages of both groups C and E varied considerably. Like group B, the maximum percentages for group C decreased and moved toward smaller diameters with increasing wind velocity. This was because the Stokes number increased with increasing wind velocity, which made it more difficult for a larger rebounding particle to follow the airflow through an orifice. In contrast, group E contains a small portion of particles for diameters below 17 μm but considerably increased portions for larger particles, as shown by the "S" shaped curves. For a given particle size, the percentage increased with increasing wind velocity because a higher inertia resulted in less chance for the rebounding particle to enter an orifice. In general, group C mainly consists of particles that impacted a blunt surface not far away from the central axis of the sampler, while group E consists of particles that impacted a blunt surface near the sampler's edge.

Combining groups C and E, the percentage of particles that impacted the blunt surfaces was as high as about 80% for diameters >30 μm. This was about the same as the percentage of the blunt surface across the sampling plane. However, one can see that the prediction of group C or E particles would be greatly influenced by the accuracy of the specified coefficient of restitution, the difference in orifice distributions between the button sampler and the numerical model, and possibly other factors. It is postulated that group C particle trajectories would be overestimated in this model compared to the button sampler since a rebounding particle would have a higher probability of being collected through a circular slit than through a tiny hole, whereas group E was likely to be underestimated since a smooth and clean surface in the numerical model would promote multiple impacts that would allow a particle to move toward the sampler's edge or bypass the sampler. These are the reasons that k_1 and k_2 were introduced in Equation (3). Although the probability for group A might be overestimated similar to group C due to the difference in the orifice distributions between this model and the button sampler, the magnitude was expected to be much smaller because group C involved multiple impacts that enhanced the problem. Therefore we ignored the correction for group A in the calculations of sampling efficiency.

The smallest portion among the 5 groups was group D, as shown in Figure 8d. As stated earlier, this group contains particles that impacted a blunt surface, bounced, and ultimately came to rest on a surface. Although there was not as clear a pattern of the effects of wind velocity as exhibited in the other groups, it is evident that particle sizes around 10 μm had the highest chance to do so. For the smallest particle size simulated, i.e., 5 μm, the percentages increased with increasing wind velocity (most of the rest of the 5 μm particles were categorized into group A). This is because the rebound for such small particles was dominated by the critical impact velocity that was increased with decreasing particle size (Wall et al. 1990). For larger particles, however, an opposite pattern was observed, because critical impact velocity was not important for their rebound.

Sampling Efficiencies

Sampling efficiencies were calculated based on the particle trajectory information. The values of k_1 and k_2 in Equation (3) were first fitted to the experimental sampling efficiencies using the minimizing program MINUIT (James and Roos 1975). The best-fit values of k_1 and k_2 were 0.378 ± 0.034 and 0.793 ± 0.023 (one standard deviation), respectively, with a correlation coefficient of 0.302 between k_1 and k_2 (the p-value of the fit was 0.62). The results imply that only about 40% of group C particles could actually bounce inside the sampler, while about 80% of group E particles could actually bypass the sampler (the other

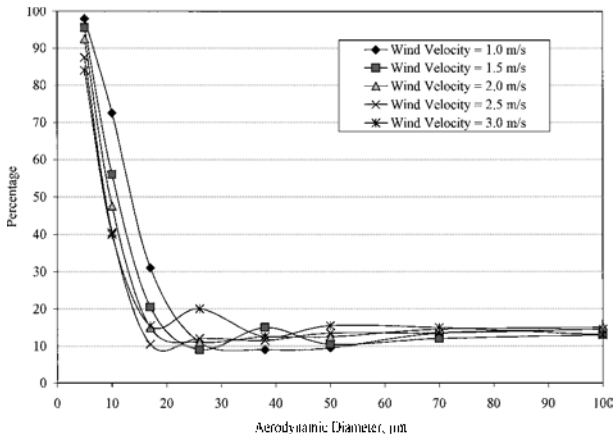

(*a*)

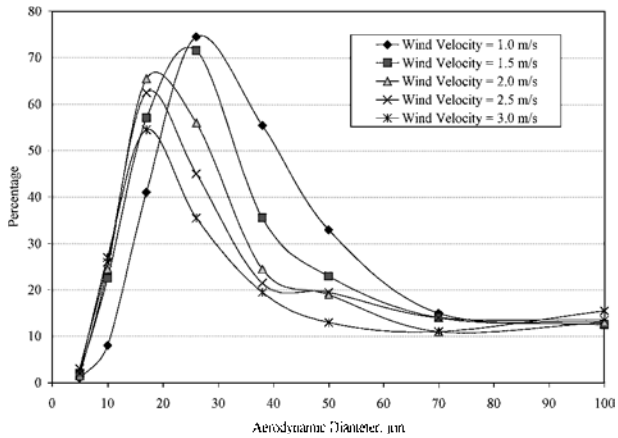

(*c*)

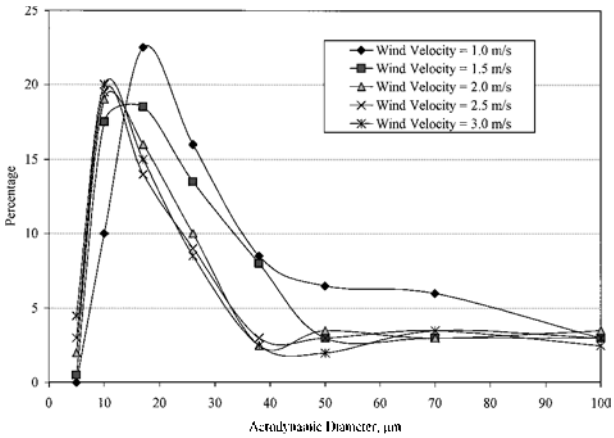

(*b*)

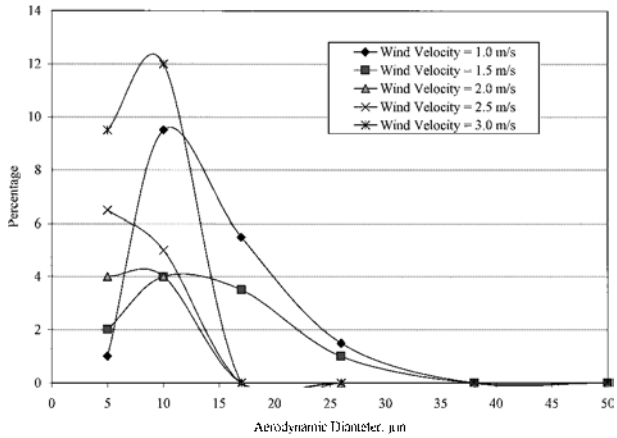

(*d*)

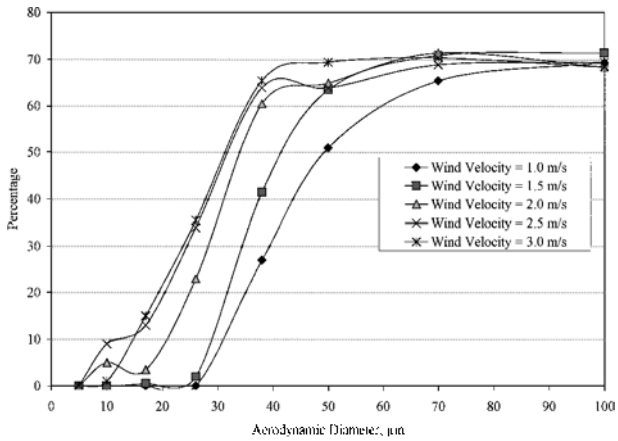

(*e*)

Figure 8. Detailed information on particle trajectories comprising 5 groups: (a) group A, (b) group B, (c) group C, (d) group D, and (e) group E.

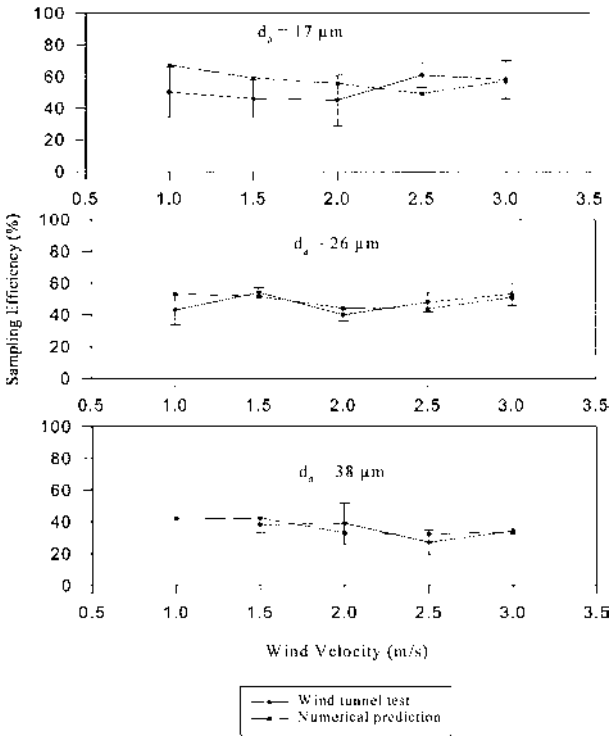

Figure 9. Comparison of numerical results from the simplified model with the experimental data for the button sampler at aerodynamic diameters of 17, 26, and 38 μm, respectively. The values of k_1 and k_2 were thus estimated to be 0.378 and 0.793, respectively. The error bars indicate the standard deviation of the overall sampling efficiency to the mean of each set of results.

20% could bounce inside the sampler) based on the experimental data. Figure 9 is a comparison of the numerical results from the simplified model with the experimental data for the button sampler. The error bars indicate the standard deviation of the overall sampling efficiency to the mean of each set of results.

Using the values of k_1 and k_2, sampling efficiencies predictions for the button sampler were then extrapolated to the sizes that cover the entire ACGIH inhalability curve. Figure 10 shows the predicted sampling efficiencies for solid particles at wind velocities ranging from 1.0 to 3.0 m/s. Generally, efficiencies decreased with increasing particle size up to approximately 40 μm and then remained virtually unchanged up to 100 μm at about 35%. Although the predicted efficiencies of the first prototype of the button sampler were generally lower than the ACGIH inhalability curve for particle sizes >15 μm, both exhibited a quite similar pattern. Figure 10 also demonstrates that the effect of the wind velocity on the sampling efficiency was small. For particles smaller than about 45 μm, sampling efficiency slightly decreased with increasing wind velocity, while an opposite trend was observed for the larger particles, except for the low wind velocity of 1.0 m/s. This crossover phenomenon was also observed for the IOM static inhalable aerosol sampler, with the crossover point also around 45 μm (Vincent 1994). It is postulated that

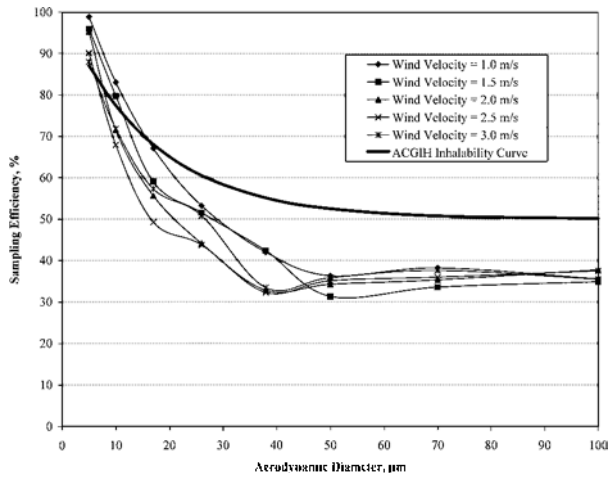

Figure 10. Numerical predictions (with 2 fitted parameters) of sampling efficiencies for solid aerosol particles.

the inhalable convention could be nearly matched by increasing the following design parameters: inlet porosity, orifice diameter, sampling flow rate, or a combination of these. As shown in the recent experimental study by Aizenberg et al. (2000), the sampling efficiency of the current version of the button sampler having a larger orifice diameter (381 μm), greater inlet porosity (21%), and higher sampling flow rate (4 L/min) appeared to be slightly higher than the one observed experimentally and theoretically for the first prototype.

Sampling efficiencies for liquid aerosols were also predicted by letting $k_1 = 0$ and $k_2 = 1$ in Equation (3). By including all the group B particles in the numerical estimate, the assumption is being made that all but an insignificant fraction of the particles that hit the side wall of such a small orifice are eventually collected on the filter. As shown in Figure 11, the patterns of the sampling efficiencies were quite similar to those exhibited in Figure 10. Efficiencies for particles smaller than 10 μm were

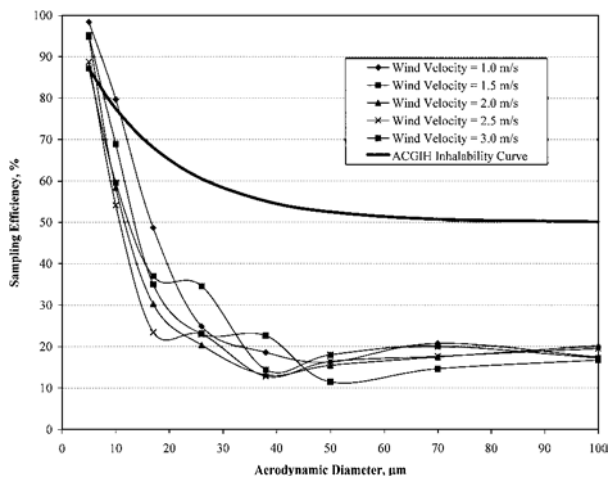

Figure 11. Numerical predictions of sampling efficiencies for liquid aerosol particles.

not significantly different from solid particles. However, the efficiencies were noticeably lower than those for solid particles for larger particles. Therefore, it is postulated that a different design is needed for liquid aerosols in order to approach the same sampling convention.

SUMMARY AND CONCLUSIONS

The performance of an aerosol sampler with a curved, blunt, multi-orificed inlet was numerically evaluated by CFD. Experimental data in sampling efficiency of the button sampler (the first prototype) for 3 particle sizes were used to approximate the interactions between the particle and the blunt surfaces at the inlet surface. Details in flow fields and particle trajectories revealed the physics of the sampler performance.

Numerical simulations were carried out under a variety of wind velocities, ranging from 0.5 to 4.0 m/s, with the sampler facing the wind. The model revealed that the multi-orificed curved surface played an important role in equalizing internal pressure variation, thus reducing the wind effect and offering virtually uniform deposition of particles on the filter. Uniformity of particle deposition on the filter declined with increasing particle size and wind velocity. At a high velocity, uniformity could be improved by increasing the sampling flow rate.

Sampling efficiencies were predicted for the button sampler for solid particle sizes between 5 and 100 μm. Efficiency gradually decreased with increasing particle size up to about 40 μm and then remained virtually unchanged at about 35%. The trend of the efficiency curve was similar to the ACGIH inhalability curve in spite of being slightly lower for larger particles. Sampling efficiencies of an aerosol sampler with a curved, blunt, multi-orificed inlet for liquid aerosol particles larger than 15 μm were predicted to be significantly lower than those for solid particles.

The simplification of the sampler's geometry in the CFD model reduced the uniformity of the orifice distribution across the sampling surface. This was expected to have an effect on the calculated particle trajectories because of a change of the probability that a particle would directly pass through an orifice or hit a wall. However, the physics of the performance of the sampler and the main conclusions for the sampling efficiency derived from this study are expected to be valid.

Significant phenomena in the innovative design of the button sampler include the advantages of relatively uniform filter deposition and low dependence on wind speed and the disadvantages of high impaction rates for relatively large particles on the inlet surface (with bounce for solid particles) and the possibility of flow out of the orifices near the edge if the sampling flow is too low for the ambient wind speed.

REFERENCES

Aizenberg, V., Bidinger, E., Grinshpun, S. A., Willeke, K., Hamed, A., and Tabakoff, W. (1998). Airflow and Particle Velocities Near a Personal Aerosol Sampler with a Curved, Porous Aerosol Sampling Surface, *Aerosol Sci. Technol.* 28:247–258.

Aizenberg, V., Grinshpun, S. A., Willeke, K., Smith, J., and Baron, P. A. (2000). Performance Characteristics of the Button Personal Inhalable Aerosol Sampler, *Am. Ind. Hyg. Assoc. J.* 61:398–404.

American Conference of Governmental Industrial Hygienists (1998). *TLVs® and BEIs®, Threshold Limit Values for Chemical Substances and Physical Agents and Biological Exposure Indices*, Cincinnati, OH.

Baron, P. (1998). Personal Aerosol Sampler Design: A Review, *Appl. Occup. Environ. Hyg.* 13:313–320.

Berry, R. R., and Froude, S. (1989). *An Investigation of Wind Conditions in the Workplace to Assess Their Affect on the Quantity of Dust Inhaled*, Health and Safety Executive Report, IR/L/DS/89/3, Health and Safety Executive, London.

Brach, R. M., and Dunn, P. F. (1998). Models of Rebound and Capture for Oblique Microparticle Impacts, *Aerosol Sci. Technol.* 29:379–388.

Engelman, M. S. (1993). *FIDAP Theory Manual*, Version 7.0, Fluid Dynamics International.

Gao, P., Dillon, H. K., Baker, J., and Oestenstad, K. (1999). Numerical Prediction of the Performance of a Manifold Sampler with a Circular Slit Inlet in Turbulent Flow, *J. Aerosol Sci.* 30:299–312.

Griffiths, W. D., and Boysan, F. (1996). Computational Fluid Dynamics (CFD) and Empirical Modeling of the Performance of a Number of Cyclone Samplers, *J. Aerosol Sci.* 27:281–304.

Grinshpun, S., Aizenberg, V., Reponen, T., Wang, Z., Gorny, R., and Willeke, K. (2000). *Performance of the Button Sampler for Total and Viable Enumeration of Airborne Microorganisms*, American Industrial Hygiene Conference & Exposition, Orlando, FL, May 20–25, 2000.

Hauck, B. C., Grinshpun, S. A., Reponen, A., Reponen, T., Willeke, K., and Bornschein, R. L. (1997). Field Testing of New Aerosol Sampling Method with a Porous Curved Surface as Inlet, *Am. Ind. Hyg. Assoc. J.* 58:713–719.

International Standards Organization (ISO) (1991). *Air Quality—Particle Size Fraction Definitions for Health-Related Sampling*, Approved for Publication as CD 7708, ISO, Geneva.

James, F., and Roos, M. (1975). MINUIT—A System for Function Minimization and Analysis of the Parameter Errors and Correlations, *Comput. Phys. Commun.* 10:343–367.

Kalatoor, S., Grinshpun, S. A., Willeke, K., and Baron, P. (1995). New Aerosol Sampler with Low Wind Sensitivity and Good Filter Collection Uniformity, *Atmos. Environ.* 29:1105–1112.

Katz, I. M., Davis, B. M., and Martonen, T. B. (1999). A Numerical Study of Particle Motion within the Human Larynx and Trachea, *J. Aerosol Sci.* 30:173–183.

Kulmala, I. K. (1997). Air Flow Field Near a Welding Exhaust Hood, *Appl. Occup. Environ. Hyg.* 12:101–104.

Li, W. I., Perzl, M., Ferron, G. A., Batycky, R., Heyder, J., and Edwards, D. A. (1998). The Macrotransport Properties of Aerosol Particles in the Human Oral-Pharyngeal Region, *J. Aerosol Sci.* 29:995–1010.

Rao, N. P., Navascues, J., and Fernadez de la Mora, J. (1993). Aerodynamic Focusing of Particles in Viscous Jets, *J. Aerosol Sci.* 24:879–892.

Soderholm, S. C. (1989). Proposed International Conventions for Particle Size-Selective Sampling, *Ann. Occup. Hyg.* 33:301–320.

Tu, J. Y. (2000). Numerical Investigation of Particulate Flow Behavior in Particle-Wall Impaction, *Aerosol Sci. Technol.* 32:509–526.

Twohy, C. H. (1998). Model Calculations and Wind Tunnel Testing of an Isokinetic Shroud for High-Speed Sampling, *Aerosol Sci. Technol.* 29:261–280.

Vincent, J. H. (1989). *Aerosol Sampling–Science and Practice*, John Wiley and Sons, New York, pp. 100, 102, 128, and 220.

Vincent, J. H. (1994). Measurement of Coarse Aerosols in Workplace–A Review, *Analyst* 119:13–18.

Wall, S., John, W., and Wang, H.-C. (1990). Measurements of Kinetic Energy Loss for Particles Impacting Surfaces, *Aerosol Sci. Technol.* 12:926–946.

Whitby, E. R. (1989). *Modal Aerosol Dynamics Modeling*, Ph.D. thesis, University of Minnesota, Minneapolis, MN.

Wilck, M., and Stratmann, F. (1997). A 2-D Multicomponent Modal Aerosol Model and its Application to Laminar Flow Reactors, *J. Aerosol Sci.* 28:957–972.